Numerical Simulation of Airflow over Mountains

Israel G. Bentillo, Ph. D.
Associate Professor of Meteorology
University of the Philippines
Diliman, Quezon City

ABSTRACT

This paper presents a primitive-equation two-dimensional mesoscale model which simulates orographic airflow using meteorological variables which are routinely observed from a single radiosonde station and yields wind velocities at about 4-km grid spacing as output. The model components representing the subgrid planetary boundary layer processes are parameterized by bulk physical methods and the resulting closed set of prognostic and diagnostic equations are integrated numerically by a semi-implicit scheme.

Numerical experiments were conducted to test the ability of the model to simulate airflow over theoretical and actual terrains. The first experiment was done on a 1-km bell-shaped theoretical mountain while the second was made using the idealized profile of the Colorado Rockies where sufficient observational data were available. Model runs were also done on actual terrain of Sierra Nevada mountains and Benguet-Ifugao mountains. The results of the experiments showed that mean large-scale flow of 20 m/s could accelerate to as much as 32 m/s for a 1-km mountain and 45 m/s for a 2-km mountain. The maximum horizontal velocities occurred at the lee side of the mountains at about 1 km above ground. The vertical wind velocity structure showed maximum descent of about 300 cm/s at the lee side at low levels. The cells of

maxima and minima tilted slightly upstream in good qualitative agreement with the classical theory of hydrostatic mountain waves.

It is concluded that the model is capable of simulating wind flow with enough accuracy to justify its use for studies such as atmospheric pollution, wind energy prospecting, aviation safety, cloud seeding, and mesoscale orographic rainfall prediction.

INTRODUCTION

The numerical simulation of airflow over complex terrains continues to be one of the most challenging subjects in dynamic meteorology today. While scientific curiosity is a legitimate motivation for numerical experiments on mesoscale wind fields, applications of the results of such studies are numerous. Some of the most important application areas are in the fields of atmospheric pollution transport modelling, watershed rainfall prediction, wind energy development, weather modification, and studies on air navigation safety.

Early theoretical studies of air flow over mountains were conducted using linear models such as those by Queney (1948) and Scorer (1949). In more recent years, nonlinear numerical models have been developed by Estoque (1963), Hovermale (1965), Mahrer *et al.* (1975), Deavaen (1976), Klemp *et al.* (1978), Anthes *et al.* (1978), and Nickerson *et al.* (1986).

In this paper a nonlinear numerical model is presented. This model requires upper air observations at an upstream radiosonde station as input and yields horizontal and vertical wind fields at about 4 km resolution. The set of governing equations used includes the equation of motion, continuity equation, thermodynamic energy equation, hydrostatic equation and first-order closure equations for boundary layer parameterization. The coordinate system used is similar to that of the sigma coordinate system described by Mahrer and Pielke (1975).

The basic assumptions made in the conception of the model are that terrain-induced wind system responds determinastically with the prevailing synoptic scale flow pattern and that the mesoscale system quickly adjusts to the synoptic scale conditions in at least a quasi-steady balance.

The numerical experiments were done using theoretical and actual mountains.

MODEL EQUATIONS

The formulation of the model equations and the transformation of these equations to the sigma coordinate system is described in detail by Bentillo (1989). Using symbols listed in the Appendix, the model equations can be written as

Horizontal Equations of Motion

$$\frac{\partial u}{\partial t} = -u\frac{\partial u}{\partial x} - \omega\frac{\partial u}{\partial \sigma} fv - \theta\frac{\partial \pi}{\partial x} - g\frac{D-\sigma}{D}\frac{\partial h}{\partial x} + \frac{D}{\rho_o (D-h)}\frac{\partial \tau_u}{\partial \sigma} \quad (1)$$

$$\frac{\partial v}{\partial t} = -u\frac{\partial v}{\partial x} - \omega\frac{\partial v}{\partial \sigma} - fu + fu_g + \frac{D}{\rho_o (D-h)}\frac{\partial \tau_v}{\partial \sigma} - \quad (2)$$

Continuity Equation

$$\frac{\partial (\rho_o \omega)}{\partial \sigma} = -\frac{\partial (\rho_o u)}{\partial x} + \frac{\rho_o u}{D-h}\frac{\partial h}{\partial x} \quad (3)$$

Thermodynamic Energy Equation

$$\frac{\partial \theta}{\partial t} = -u\frac{\partial \theta}{\partial x} - \omega\frac{\partial \theta}{\partial \sigma} \quad (4)$$

Hydrostatic Equation

$$\frac{\partial \pi}{\partial \sigma} = \frac{D-h}{D}\frac{g}{\theta} \quad (5)$$

where

$$\sigma = D\frac{z-h}{D-h} \quad (6)$$

$$\omega = \frac{d\sigma}{dt} = \frac{D}{D-h}w + \frac{D-\sigma}{D-h}u\frac{\partial h}{\partial x} \quad (7)$$

$$\pi = C_p\left[\frac{p}{P_o}\right]^{\kappa} \quad (8)$$

The five dependent variables in this set of five equations are u, v, ω, θ, and π. As can be seen from the above equations, the factors affecting the values of these dependent variables and the steady-state solution of the model equations are: the terrain forcing, turbulent eddy fluxes, gravitational acceleration, coriolis acceleration, pressure gradient force, horizontal and vertical advection, and the initial conditions. Of course, unseen from the above equations are other factors which include the numerical methods, the specification of the spatial boundary conditions, terrain smoothing and the choice of the grid system.

The model assumes two dimensionality in the x-∂ plane. This assumption is dictated by computational limitations particularly the speed of computer calculations and computer storage.

TREATMENT OF VERTICAL EDDY DIFFUSION

At the surface, the vertical eddy diffusion is parameterized using drag coefficient representation as

$$\tau_{us} = \rho_s C_D \left| V_s \right| u_s \tag{9}$$

$$\tau_{vs} = \rho_s C_D \left| V_s \right| v_s \tag{10}$$

where C_D is the drag coefficient, $|\mathbb{V}|$ is the magnitude of horizontal velocity and the subscript s denotes surface values.
At levels above the surface, the stresses are represented by a mixing length formulation described in Colton. (1976) giving

$$\tau_u = \frac{D}{D-h} \rho_D K \frac{\partial u}{\partial \sigma} \tag{11}$$

$$\tau_v = \frac{D}{D-h} \rho_D K \frac{\partial v}{\partial \sigma} \tag{12}$$

where

$$K = \frac{D}{D-h} L^2 \left| \frac{\partial v}{\partial \sigma} \right| \tag{13}$$

The mixing length L is given by the formula

$$L = \kappa h_s \left[1 - \frac{\sigma}{D}\right] \tag{14}$$

where k = von Karman constant and h_s = height of the surface layer.

TREATMENT OF HORIZONTAL EDDY DIFFUSION

In this model the horizontal eddy diffusion is represented by the horizontal smoothing function by Shuman (1957) and given as

$$\bar{\phi}_i = (1 - \nu_i)\,\phi_i + \nu_i \left[\frac{\phi_{i+1} + \phi_{i-1}}{2}\right] \tag{15}$$

where ϕ_i is either u, v or θ, $\bar{\theta}_i$ is the smoothed value of θ_i and ν_i is the Shuman filter coefficient.

Mahrer and Pielke (1975) have shown by numerical experiment that this numerical smoothing technique produces a steady-state solution twice as fast as that by the use of a horizontal exchange coefficient of the form

$$K_H = \sigma (\Delta x)^2 \left[\left(\frac{\partial v}{\partial x}\right)^2 + \frac{1}{2}\left(\frac{\partial u}{\partial x}\right)^2\right]^{\frac{1}{2}} \tag{16}$$

with almost the same results.

GRID SYSTEM

A horizontally staggered grid system is used in this model. The horizontal components of velocity are defined at full grid points while the vertical velocity, potential temperature, and scaled pressure are at half grid points in the horizontal. All variables are computed at each level in the vertical.

The horizontal grid spacing is 4.3 km at the region of interest which increases exponentially near the lateral boundaries. The grid mesh consists of 49 horizontal grid points and 13 vertical sigma levels. These levels correspond to elevations of 0, 500, 1000, 2000, 3000, 4000, 5000, 6000, 7000, 8000,

9000, 10000 and 11000 m on a plain surface. The total horizontal domain is 330 km and the central region of interest is 172 km.

SEMI-IMPLICIT INTEGRATION OF MODEL EQUATIONS

The model equations are integrated using a semi-implicit scheme. In this scheme, the equations are evaluated in the following order:

a) Forecast u from the east-west momentum equation.
b) Forecast v from the north-south momentum equation using the new values of u in the coriolis term.
c) Diagnose ω from the continuity equation using new values of u.
d) Forecast θ using new values of u and ω.
e) Diagnose π for the hydrostatic equation using new values of θ.
f) Repeat the process until a quasi-steady-state solution is reached.

This scheme does not only increase linear computational stability but also reduces computer storage requirements by solving the prognostic equations sequentially.

NUMERICAL SCHEMES

The prognostic equations are integrated using a forward-upstream difference scheme for all advective terms. The remaining space derivatives are evaluated using the centered difference scheme for uneven grid distances derived from quadratic Lagrange interpolating polynomial used by Estoque (1988).

The use of the forward-upstream was recommended by Colton (1976) as well-suited for steady-state solutions due to its strong implicit diffusion although the scheme has received much criticism for the same reason. Comparison of the results of simulations of flow over Colorado Rockies by Klemp and Lilly (1978), where centered differencing scheme accurate to second-order in time and space was used, with those of Deaven (1976) and Mahrer and Pielke (1975) shows close agreement especially in locations of maxima and minima. The use of upstream cubic spline interpolating polynomial, which is more conservative than the upstream scheme, also showed similar results as can be seen in Mahrer and Pielke (1978)).

INITIALIZATION OF THE MODEL

The model can be initialized using observations from a single upwind radiosonde station. The input data consists of the synoptic-scale geostrophic winds at z-surfaces and the air temperatures at isobaric surfaces.

To transfer the temperature data to z-surfaces, the height field is computed by assuming hydrostatic balance between potential temperature and scaled pressure. Then all the input data are interpolated to sigma surfaces where the initial values of potential temperature, scaled pressure, and synoptic-scale density fields are computed. The initial field of sigma vertical velocity is assumed to be zero.

The methods of interpolation used are the Lagrange interpolation for the sigma levels adjacent to the top and bottom boundaries and the cubic spline interpolation for the rest of the interior sigma levels.

The wind field is initialized using a one dimensional form of dynamic initialization. In this method, the horizontal momentum equations are reduced to the forms in which the nonlinear terms are removed and the pressure gradient terms expressed in terms of geostrophic assumption and are given as

$$\frac{\partial u}{\partial t} = fv - fv_g + \frac{D}{\rho_o (D - h)} \frac{\partial \tau_u}{\partial \sigma} \tag{17}$$

$$\frac{\partial v}{\partial t} = fu_g - fu + \frac{D}{\rho_o (D - h)} \frac{\partial \tau_v}{\partial \sigma} \tag{18}$$

These equations express the balance between large-scale pressure gradient, coriolis, the frictional forces for a given geostraphic wind and temperature profile. The equations are then integrated in time at the radiosonde site from an initial guess fields of u and v until the changes in u and v are arbitrarily small.

The next step in the initialization is the introduction of the mountain range barrier. Deaven (1976) describes a method called diatrophism to prevent initial shock due to sudden introduction of a mountain. In this method, the lowest surface of the model is slowly transformed from the initial flat surface to the actual topography. The time rate of change of the surface is determined by trial and error. If the barrier is introduced too

fast, then the spurious accelerations and hydrostatic imbalances cause perturbations that will take much time to remove by the diffusion and implicit smoothing of the finite difference operators. This requires excessive computer time to attain a quasisteady state solution. Deaven used a growing period of 180 time steps at Δt of 20 sec. and the quasisteady state solution is obtained after 1.5 to 2 hours of model time for the Rocky mountains. In this model, the mountain is introduced linearly within the first 2 hours of simulation time - that is, 360 time steps at Δt equal to 20 sec.

BOUNDARY CONDITIONS

At the top boundary, the scaled pressure is held constant equal to its initial value; the vertical derivative of potential temperature is held constant equal to its initial value if the sigma vertical velocity is negative; and the vertical derivatives of the horizontal wind components are set equal to zero if the sigma vertical velocity is negative. At the bottom boundary the sigma vertical velocity is held constant equal to zero.

At the inflow lateral boundary, the sigma vertical velocity is set constant equal to zero and the horizontal derivatives along the x-direction is set constant equal to zero. The inflow and outflow boundaries are defined in terms of the wind direction at these boundaries.

To absorb reflections from the top of the model, a horizontal smoothing function of the form

$$\bar{\phi} = (1 - b)\ \phi_i + 0.5\, b\ (\phi_{i+1} + \phi_{i-1}) \qquad (19)$$

is applied at the topmost four levels where b varies linearly with height from zero at the bottom of the absorbing layer to 0.5 at the top of the model. Klemp and Lilly (1978) strongly suggest the necessity of this layer.

SIMULATION OF FLOW OVER A THEORETICAL RIDGE

The first numerical experiment is done on a bell-shaped theoretical ridge with the form

$$h = \frac{H_o\, B}{\left[x^2 + B^2\right]^{0.5}} \qquad (20)$$

which defines a symmetric barrier with maximum elevation of H_o and a half-width of B. This theoretical mountain has been used by Deaven (1976), Mahrer and Pielke (1975, 1978), Klemp and Lilly (1978), and Nickerson *et al* (1986) and is adopted in this study for convenience in comparison of results.

The first run is done using H_o equal to 1 km and B equal to 15 km. The initial thermodynamic conditions are identical to those of Colton (1976) shown in Fig. 1 and the initial wind profile is 20 ms^{-1} at every grid point in the model. The model is run for 7.5 hours of model time which corresponds to a nondimensional time of 18 which is larger than 16 as required by momentum flux analysis of Klemp and Lilly (1978) for 1-km mountain to reach steady state.
In this run the horizontal smoothing at the upper absorbing layer is omitted but the Shuman filter coefficient of 0.1 is used to maintain nonlinear stability.

The results of this run is shown in Fig. 2. The horizontal wind speed distribution is shown in Fig. 2a. It can be seen that the horizontal velocity has increased to about 30 meters per second at approximately 10 km to the lee velocities which is comparable to the results of Klemp and Lilly (1978) for the same height of mountain. The lee velocities are weaker at high altitudes agreeing with the observations.

The height and location of the maximum velocity, which indicates how well the momentum flux is modeled, is in good agreement with Mahrer *et al.* (1975). The magnitude of the surface winds on the windward slope decreased to about 8 m/s due to partial blocking of the low level flow by the mountain. This magnitude is comparable to the minimum surface horizontal velocities of Deaven (1976) which is 6 m/s.

The vertical velocity field (Fig. 2b) shows upward motion predominating below 5 km on the windward slopes of the barrier as expected due to the forced ascent and a general decrease of vertical velocity at higher levels on this side of the mountain due to horizontal divergence as the airflow accelerates in crossing the mountain. The maximum upward velocity at the windward side is about 1 m/s while the downward motion on the lee slope has a maximum of 2.2 m/s. Mahrer *et al.* (1975) has a maximum leeside descent of 2.2 m/s and maximum upward motion of 0.7 m/s velocity and 0.4 m/s, respectively. Mahrer and Pielke (1975) suggests that greater upward maxima can occur citing the observational studies in the Rockies which shows the existence of foehn clouds due to upward motion at the windward side under strong flow

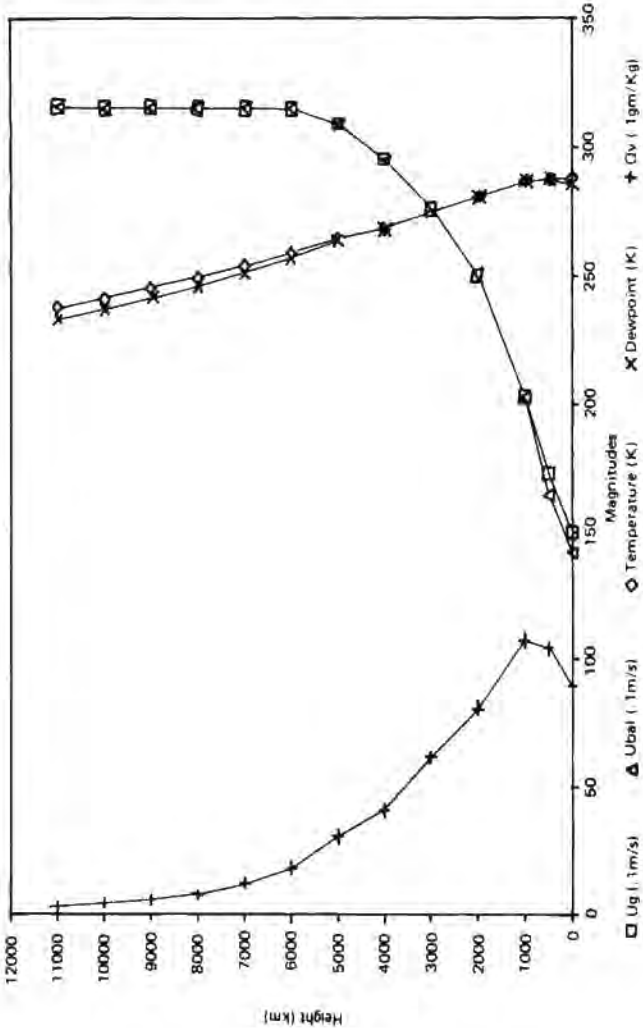

Fig. 1. Input meteorological data for the theoretical and Sierra Nevada runs.

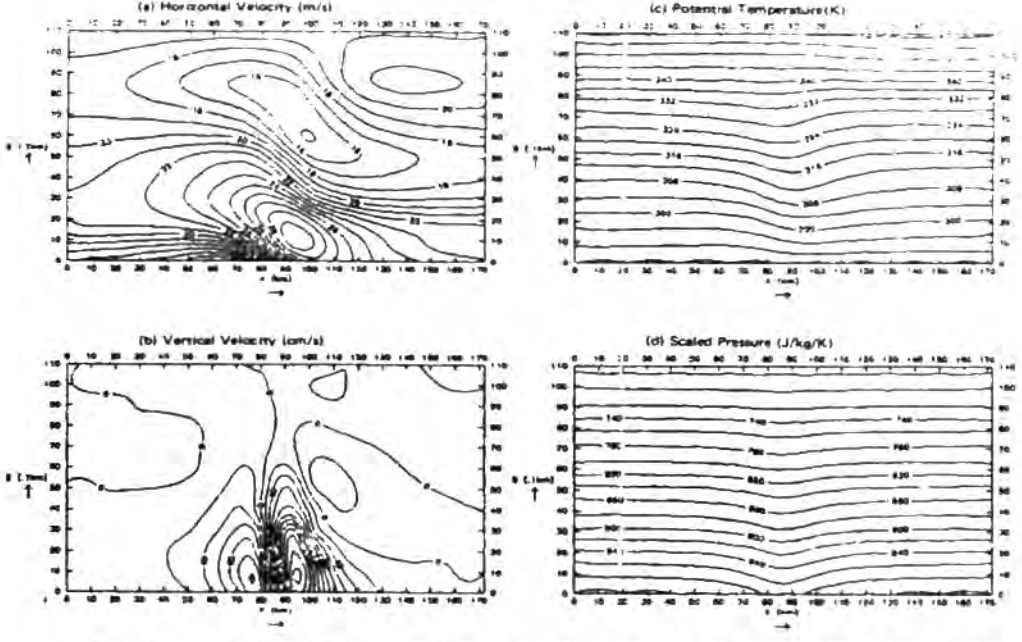

Fig. 2. Results of the 1-km theoretical mountain run plotted on sigma coordinates.

regimes. Comparison with the horizontal velocity distribution shows a negative correlation which is expected for a downward transport of momentum.

The potential temperature field (Fig. 2c) has a maximum due to adiabatic expansion as the air undergoes orographic ascent and has maximum on the leeside due to sinking. As also observed in the vertical motion filed, the maximum and minimum temperatures tilt upstream with increasing elevation in good qualitative agreement with the classical theory of two-dimensional flow over a mountain range. The amplitudes, however, are considerably damped by the strong explicit diffusion introduced in this run.

The scaled pressure field, which can be thought of as pressure since it is a function of pressure alone, is shown in Fig. 2d. This distribution is consistent with the strong convergence on the leeward slopes and strong divergence on the leeward slope at lower levels. The pressure dip from the crest to the lee slope is somewhat damped. Lilly and Zipser (1972) observed pressure dips of about 5 to 7 millibars.

The next run is done with the same initial conditions but the height of the mountain is approximately doubled to 1.9 km while the half-width is maintained at 15 km. This terrain approximates that of the Rocky Mountains west of Boulder, Colorado which is also the subject of numerical orographic airflow experiments by Mahrer *et al.* (1975, 1978), Deaven (1976), Klemp et al ('978) and others. This increase of mountain height will cause a substantial enhancement of momentum flux. Klemp and Lilly (1978) suggests a nondimensional time of 30 required before the flux profile is nearly constant with height. The nondimensional time used which 28.8 is somewhat deficient but is much higher than those used by Deaven (1976) and Pielke (1975) which are 5.4 and 7.2, respectively which Klemp and Lilly (1978) associate with still an early stage of wave development.

In this experiment, an upper layer sponge absorber in the form of smoothing is used. The Shuman filter coefficient used at the region of interest is reduced to 0.02 which is about double of that used by three dimensional models with similar values of prevailing wind, grid distance and time step. This is suggested by Pielke (1974) in his comparison study between modeling capabilities of two-dimensional and three-dimensional models in the mesoscale.

The results of the second run are shown in Fig. 3. Comparisons of these figures with those of the 1-km mountain show qualitative similarities and the main differences lie in the

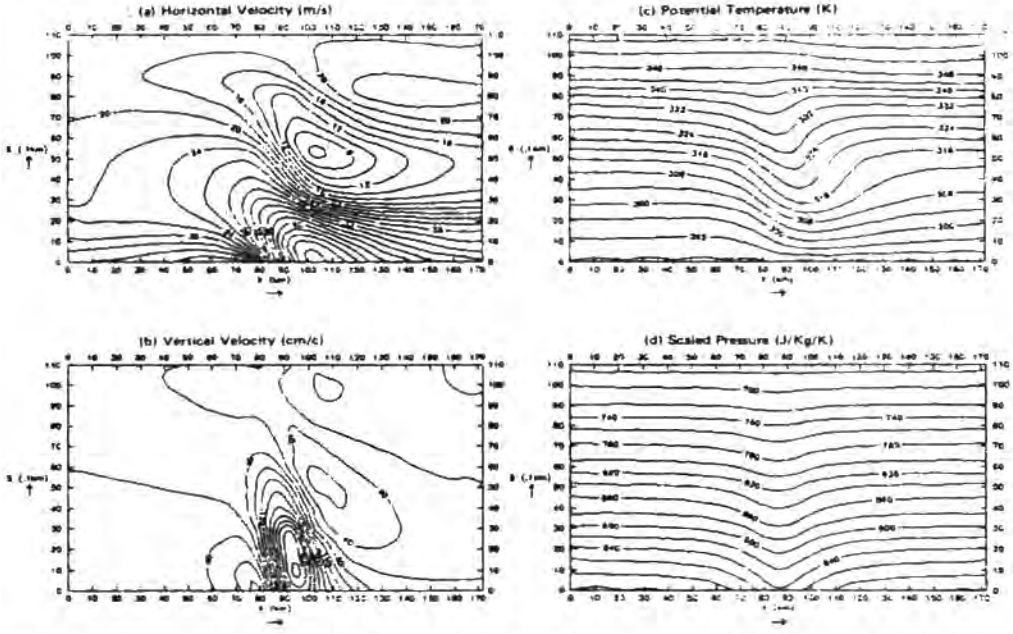

Fig. 3. Results of the 1.9-km theoretical mountain run plotted on sigma coordinates.

mum velocity at the lee slope is quite high but may not be unrealistic. In the Colorado Rockies, Danielson and Bleck (1970) reported peak velocity of 60 m/s and Lilly and Zipzer (1972) observed two severe windstorm periods in the several hours containing frequent gusts of 45 m/s with a maximum of 55 m/s. The vertical velocity maxima are increased by about fifty percent, the potential temperatures are perturbed even at higher elevations and a greater pressure dip is noticeable. An arrow plot superimposed on the vertical wind field presented in Fig. 3e shows the negative correlation between the horizontal and vertical wind fields.

SIMULATION OF AIRFLOW OVER REAL TERRAINS

The next numerical experiment was done on an actual mountain ranges. The first run used a smoothened cross section of Sierra Nevada Mountains at 30°15'00" N across the American River Basin. The choice of the area is based on data availability. The terrain and the rest of the input data for this experiment are shown in Fig. 1.

The results of this run are shown in Fig. 4. These results show the main features of the orographic flow and qualitatively similar to the dry case experiment made on the Colorado Rockies. The main difference are only due to the shape of the mountain.

In the next run, the study area is located approximately between 16° - 17°N latitudes and 120° - 121°30"E longitudes. The terrain profile passes through the province of Benguet along Dagupan-Baguio-Lagawe line. The peaks of this multimodal terrain profile are located at Mount Santo Tomas, Mount Pulog and Mount Amyao. This profile has relatively steeper slopes and higher peak.

The atmospheric dontions are represented by radiosonde data at Clark Air Base. The temperature data are shown in Fig. 5 and the wind data are presented in Fig. 6. From the temperature profiles it can be seen that the atmosphere is almost saturated and the general stability is convectively unstable below 700 mb and convectively neutral above 700 mb. The surface wind speed is 9 m/s with direction of 160° while above 1 km the wind is generally southwesterly with wind speeds of about 30-35 m/s with a maximum at 6 km. This wind profile corresponds to a strong monsoon event. Observations show that on a strong monsoon day, westerly winds stronger than 40 m/s may extend up to 10 km altitude.

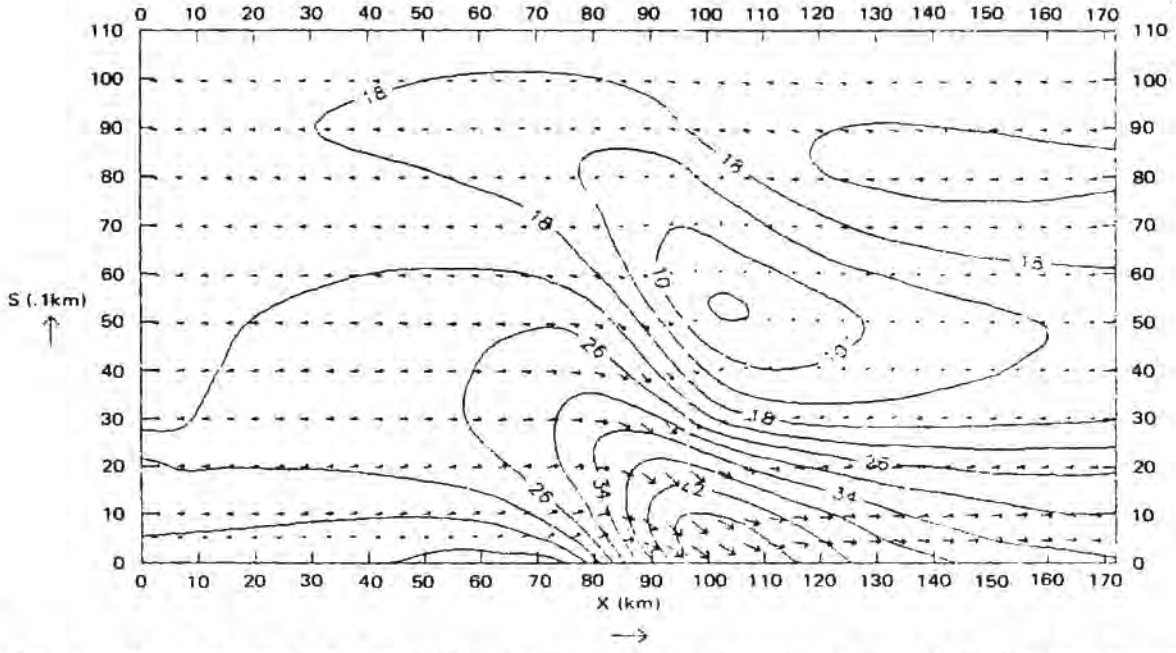

Fig. 3e. Arrow plot of the 1.9-km theoretical mountain run superimposed on lines of equal vertical velocities.

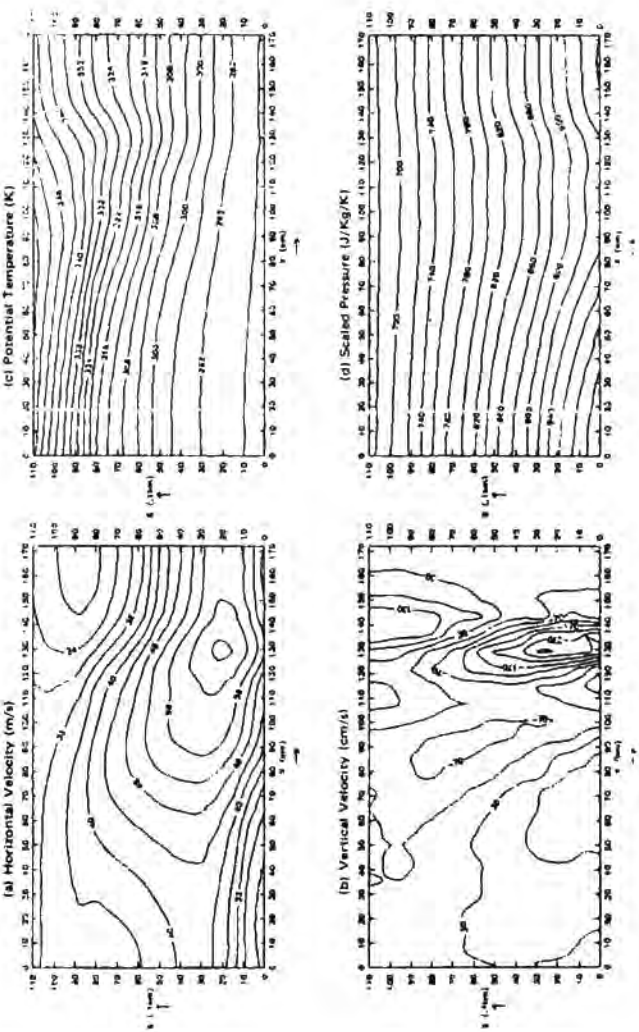

Fig. 4. Results of the Sierra Nevada run plotted on sigma coordinates.

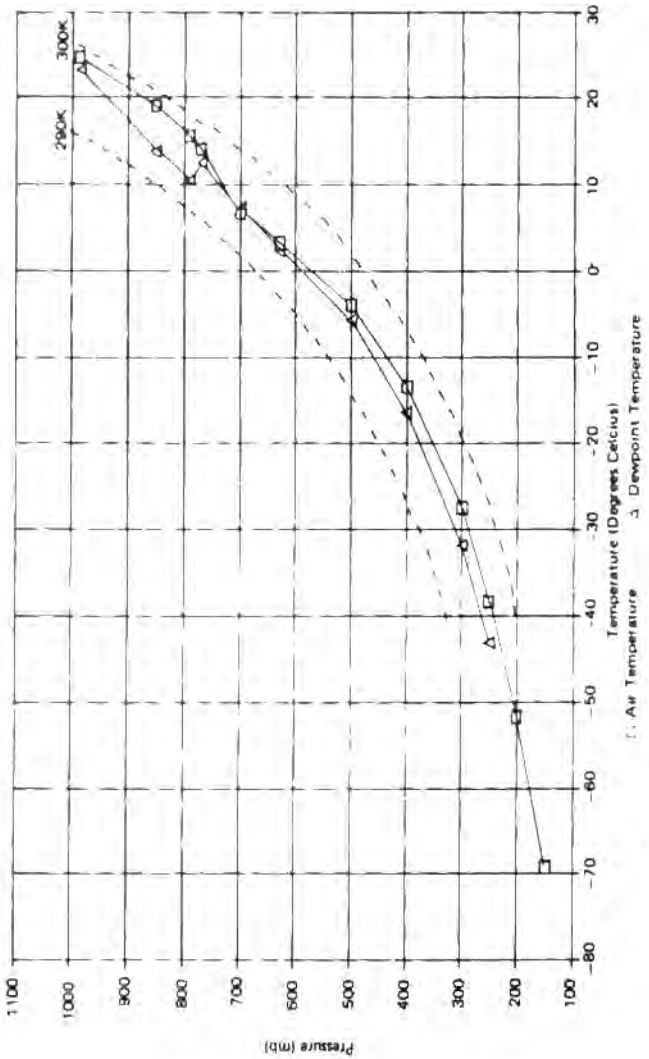

Fig. 5. Input temperature data for the Benguet-Ifugao run.

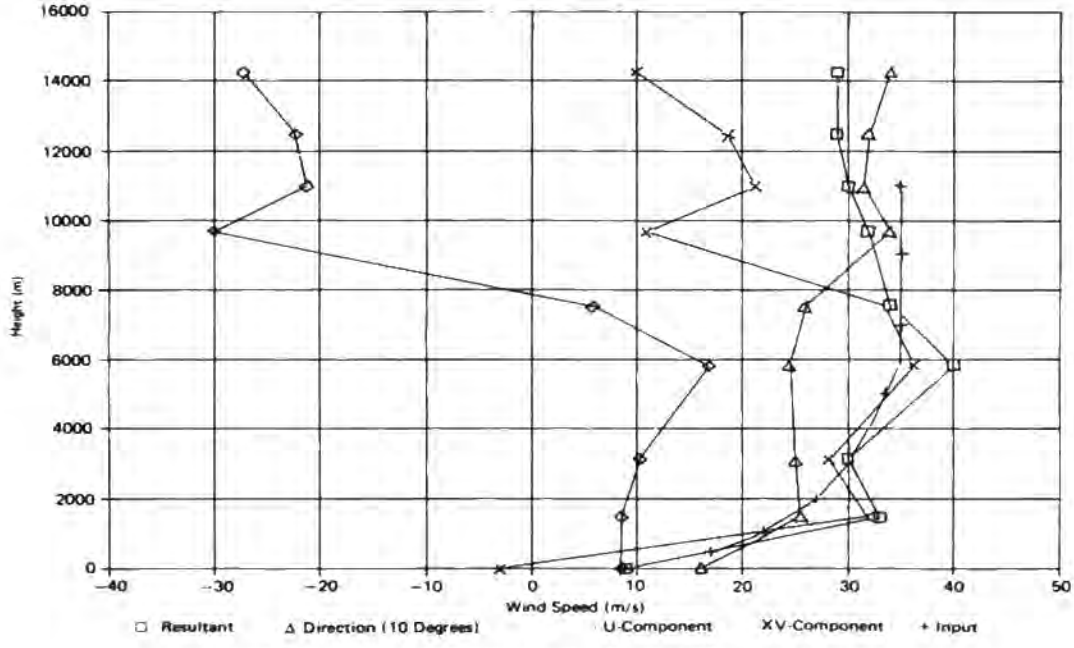

Fig. 6. Input wind data for the Benguet-Ifugao run.

The results after 12 hrs of model time is shown in Fig. 7. From Fig. 7a, it can be seen that the horizontal velocity distribution has a maximum at the lee of the ridge at about 1.8 km above the ground level. Although the magnitudes of the wind velocities are quite large due to large input values of wind speed and the higher elevation of the peak, the general distribution of the wind field agrees reasonably well with that of Sierra Nevada which has a similar profile.

The maximum updraft (Fig. 7b) of about 150 cm/s is located upwind of Mount Santo Tomas at about 32 km from Dagupan. Beyond the first peak, the vertical velocity is negative but very small in magnitude at the surface corresponding to the small descent of the terrain profile but at higher levels the downward motion is quite large with maximum of about 100 cm/flow. The next cell of upward motion with maximum of about 120 m/s extending to about 4 km is located at a distance of about 85 km corresponding to the secondary rise in the terrain towards Mount Pulog. Beyond Mount Pulog, at a distance of 105 km, a downward motion cell occurs with about 80 cm/s at the surface and 260 cm/s from 6 km upwards. The third upward motion cell is located at about 122 km as the air ascends towards Mount Amuyao with maximum of about 40 cm/s. The downward motion cell beyond Mount Amuyao is quite weaker than the previous downwad cell but the location of the maximum is closer to the surface. The general tilt of the maximum and minimum cells upstream is observed. Considering the differences in slopes and height of the ridge and the input winds, these distributions agree well with the Sierra Nevada run. These results also agree with the vertical velocity distributions of Warner *et al.* (1978).

Consistent with the distribution of vertical velocity and horizontal wind, the distributions of potential temperature and scaled pressure (Fig. 7c and 7d) have three maxima and minima. The potential temperature field generally decreases towards the right consistent with the terrain elevations. The pressure distribution is consistent with the elevations and the effects of flow dynamics which decreases pressures at the lee of the peaks.

CONCLUSION

In this study the airflow over a complex terrain is simulated during a numerical primitive-equation mesoscale model where the planetary layer processes are represented by bulk parameterization. The treatment is two-dimensional, although the formulation can easily be extended to three-dimensions. The model performs quite well and therefore may be used to

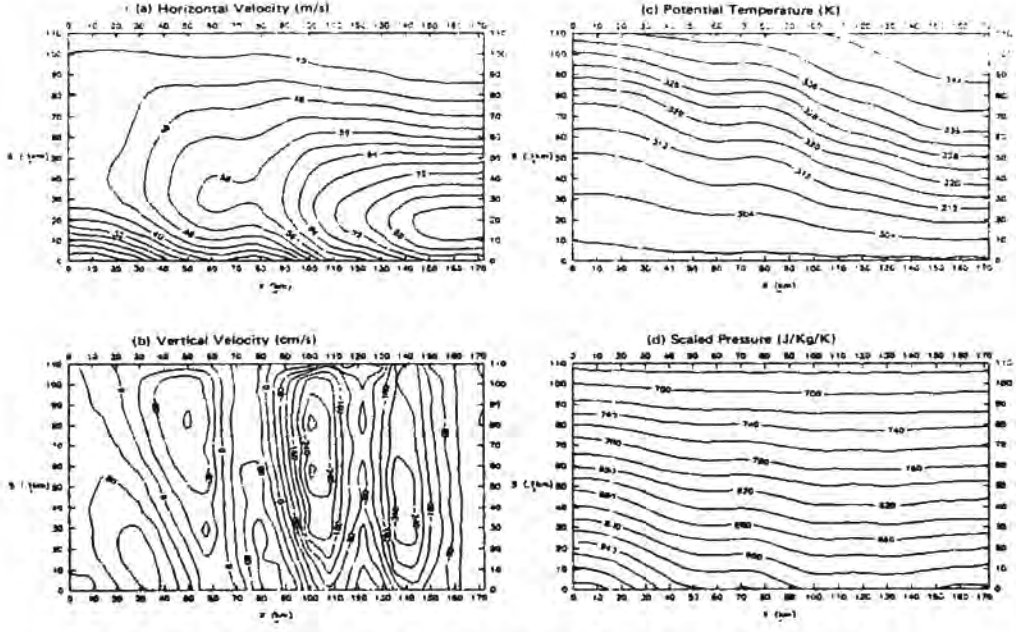

Fig. 7. Results of the Benguet-Ifugao run plotted on sigma coordinate.

provide input to other applications such as the Lagrangian dispersion model for air pollution studies.

The chief drawback of this study is its two dimensionality which prevents the model from representing three dimensional features such as flow around the barrier, convergence due to narrowing channels and variations of the shape and size of the barrier in the direction perpendicular to the flow. However, a three-dimensional treatment of this problem in the present scale requires greater machine storage capacity than is available to us.

Another numerical problem is the treatment of the top boundary reflection. The introduction of a superimposed upper isothermal damping layer which extends to about 20 km in the stratosphere as done in Klemp and Lilly (1978), Nickerson *et al.* (1976), and Mahrer and Pielke (1978) are simple to apply but will cost a lot of integration time and machine storage.

Furthermore, in order to make this model more general and applicable to different locations other mesoscale effects, such as those of the coastlines, may be incorporated. Surface heating may also be introduced for a more realistic treatment of the mountain as an elevated heat source.

LIST OF SYMBOLS

C_D	Drag coefficient
C_p	Specific heat of air at constant pressure
D	Model depth (11 km)
f	Coriolis parameter
g	Gravitational acceleration
h	Terrain height
h_s	Depth of the surface layer
K	Vertical eddy diffusion coefficent
L	mixing length
p	pressure
p_o	Reference pressure (100 000 Pa)
t	Model integration time
t'	Nondimensional time (tu/2B)
u	East-west component of horizontal velocity
V	Resultant horizontal velocity
v	North-south component of horizontal velocity
w	Cartesian vertical velocity
z	Cartesian vertical coordinate
χ	R/C_p

π Exner's function (also called Scaled Pressure)
θ Potential Temperature
ρ_o Synoptic-scale reference values of density profile
σ Terrain-following vertical coordinate
τ_u Vertical eddy stress due to vertical shear in u
τ_v Vertical eddy stress due to vertical shear in v
ω Sigma vertical velocity (da/dt)

REFERENCES

Anthes, R. and T. Warner. 1978. Development of Hydrodynamic Models Suitable for Air Pollution and Other Mesometeorological Studies. *Monthly Weather* Review, 106, 818-820

Bentillo, I. G. 1989. Numerical Simulation of Orographic Rainfall for Use in Hydrological Modelling. Ph.D. Dissertation. University of the Philippines, Diliman, Quezon City, 137 pp.

Colton, D. 1976. Numerical Simulation of the Orographically Induced Precipitation Distribution for Use in Hydrological Analysis, *Journal of Applied Meteorology*, 15, 1241-1251.

Danielson, E. F. and R. Bleck. 1970. Tropospheric and Stratospheric Ducting of Stationary Mountain Waves. Journal of *Atmospheric Science*, 27, 758-772.

Deaven, D. 1976. A Solution for the Boundary Problems in Isentropic Coordinate Models. *Journal of Atmospheric Science*, 33, 1702-1713.

Estoque, M. A. 1963. A Numerical model of the Atmospheric Boundary Layer. *Journal of Geophysical Research*, 68, 1103-1113.

Estoque, M. A. 1988. A Surface Mesoscale Wind Model for Complex Terrain. M. A. 1988. A Surface Mesoscale Wind Model for Complex Terrain. Preprint. Department of Meteorology and Oceanography, University of the Philippines. 20 pp.

Hovermale, J. B. 1965. A Non-linear Treatment of the Problem of Airflow Over Mountains. Ph.D. Dissertation. Pennsylvania State University. 88 pp.

Klemp, J. and D. Lilly. 1978. Numerical Simulation of Hydrostatic Mountain Waves. *Journal of Atmospheric Science*, 35, 78-107.

Lilly, D. K. and E. J. Zipser. 1972. The Front Range Windstorm of 11 January 1972: A Meteorological Narrative. *Weatherwise*, 25, 56-63.

Mahrer, Y. and R. Pielke. 1975. A Numerical Study of the Airflow Over Mountains Using Two-Dimensional Version of the UV Mesoscale Model. *Journal of Atmospheric Science* 32, 2144-2155.

Mahrer, Y and R. Pielke. 1978. A Test of an Upstream Spline Interpolation Technique for the Advective Terms in a Numerical Mesoscale Model. *Monthly Weather Review*, 106, 818-820.

Nickerson, E., E. Richard, R. Rosset and D. Smith. 1986. The Numerical Simulation of Clouds, Rain, and Airflow Over the Vosges and Black Forest Mountains. *Monthly Weather Review*, 114, 398-414.

Pielke, R. 1974. A Comparison of Three-Dimensional and Two-Dimensional Numerical Predictions of Sea Breezes. *Journal of Atmospheric Science*. 31, 1577-1585.

Queney, P. 1948. The Problem of Airflow Over Mountains: A Summary of Theoretical Studies. *Bulletin of American Meteorological Society*, 29, 16-26.

Scorer, R. 1949. Theory of Waves in the Lee of Mountains. *Quarterly Journal of the Royal Meteorological Society*, 75, 41-56.

Shuman, F. G. 1957. Numerical Methods in Weather Prediction: II. Smoothing and Filtering. *Monthly Weather Review*, 85, 357-361.

Vergeiner, I. 1971. An Operational Linear Lee Wave Model for Arbitrary Basic Flow and Two-Dimensional Orography. *Quarterly Journal of the Royal Meterological Society*, 97, 30-60.

Warner, T., R. Anthes, and A. McNab. 1978. Numerical Simulation with a 3-D Mesoscale Model. *Monthly Weather Review*, 106, 1079-1099.